High-Resolution Phase-Contrast Imaging of Submicron Particles in Unstained Lung Tissue

Schittny, J C ; Barré, S F ; Mokso, R ; Haberthür, D ; Semmler-Behnke, M ; Kreyling, W G ; Tsuda, A ; Stampanoni, M

DOI: https://doi.org/10.1063/1.3625383

HighResolution PhaseContrast Imaging of Submicron Particles in Unstained Lung Tissue

J. C. Schittny, S. F. Barré, R. Mokso, D. Haberthür, M. SemmlerBehnke et al.

Citation: AIP Conf. Proc. **1365**, 384 (2011); doi: 10.1063/1.3625383
View online: http://dx.doi.org/10.1063/1.3625383
View Table of Contents: http://proceedings.aip.org/dbt/dbt.jsp?KEY=APCPCS&Volume=1365&Issue=1
Published by the American Institute of Physics.

High-Resolution Phase-Contrast Imaging of Submicron Particles in Unstained Lung Tissue

J. C. Schittny[a], S. F. Barré[a], R. Mokso[b], D. Haberthür[a], M. Semmler-Behnke[c], W. G. Kreyling[c], A. Tsuda[d], and M. Stampanoni[b,e]

[a]*Institute of Anatomy, University of Bern, Baltzerstrasse 2, CH-3012 Bern, Switzerland*
[b]*Swiss Light Source, Paul Scherrer Institut, WBBA/216, CH-5232 Villigen, Switzerland*
[c]*Institute of Lung Biology, Helmholtz Center Munich, Ingolstädter Landstraße 1, D-85764 Neuherberg, Germany*
[d]*Dept. of Environmental Health, Harvard School of Public Health, 677 Huntington Ave., Boston, MA 02115, USA*
[e]*Institute for Biomedical Engineering, University and ETH Zürich, Gloriastrasse 35, 8092 Zürich, Switzerland*

Abstract. To access the risks and chances of deposition of submicron particles in the gas-exchange area of the lung, a precise three-dimensional (3D)-localization of the sites of deposition is essential—especially because local peaks of deposition are expected in the acinar tree and in individual alveoli. In this study we developed the workflow for such an investigation. We administered 200-nm gold particles to young adult rats by intratracheal instillation. After fixation and paraffin embedding, their lungs were imaged unstained using synchrotron radiation x-ray tomographic microscopy (SRXTM) at the beamline TOMCAT (Swiss Light Source, Villigen, Switzerland) at sample detector distances of 2.5 mm (absorption contrast) and of 52.5 mm (phase contrast). A segmentation based on a global threshold of grey levels was successfully done on absorption-contrast images for the gold and on the phase-contrast images for the tissue. The smallest spots containing gold possessed a size of 1-2 voxels of 370-nm side length. We conclude that a combination of phase and absorption contrast SRXTM imaging is necessary to obtain the correct segmentation of both tissue and gold particles. This method will be used for the 3D localization of deposited particles in the gas-exchange area of the lung.

Keywords: Synchrotron, x-ray tomographic microscopy, lung, submicron particles, phase contrast, absorption contrast
PACS: 68.37.Yz, 62.23.Pq, 87.57.Q-

INTRODUCTION

The use of nanomaterials is constantly increasing, be it in future technologies or in medicine. If nanomaterials are inhaled, parts will be deposited in the lung, which may lead to toxic effects. In medicine therapeutic nanoparticles should be delivered not only at the right mean concentration, but also at the right local concentration. While deposited nanomedicine may be toxic at local hotspots, the desired effect may not be achieved at local lows.

The gas-exchange area represents the most fragile part of the lung. It is organized into small, ball-like alveoli whose openings face the gas-exchanging airways. Little is known about the patterns of particle deposition. It was observed that short-term exposures to high doses of environmental air particles caused an inflammation of the gas-exchange area in normal rats [1]. However, it turned out that the centriacinar regions (region at the entrance of the gas-exchange area) were more affected than the peripheral regions [1]. Similar findings were made in neonatal rats [2]. This result was supported by numerical simulations where a higher deposition of particles was predicted in the centriacinar regions as compared to the periphery [3-5]. Furthermore, it was predicted that the pattern of particle deposition is also dependent on the size of the particles. While particles greater than 100-nm diameter are predicted to have alveolar hotspots of high depositions, smaller particles are expected to show an even distribution [6, 7].

The 10th International Conference on X-ray Microscopy
AIP Conf. Proc. 1365, 384-387 (2011); doi: 10.1063/1.3625383

To the best of our knowledge the distribution patterns of deposited submicron particles was never studied at sub-alveolar resolution due to the lack of suitable high-resolution three-dimensional (3D)-visualization methods. Our aim was to fill this gap by using synchrotron-radiation-based x-ray tomographic microscopy (SRXTM).

MATERIALS AND METHODS

Young adult WKY/Kyo@Rj rats (Janvier, Le Genest Saint Isle, France, ~ 250 g body weight) received an intratracheal instillation of a suspension of 200-nm gold particles in water after they were anesthetized by inhalation of 5% isoflurane. Thirty minutes later the lungs were fixed with 2.5 % glutaraldehyde by vascular perfusion [8], removed, and processed for paraffin embedding as described recently [9, 10]. All experiments were conducted under German federal guidelines for the use and care of laboratory animals and were approved by the Government of the District of Upper Bavaria and by the Institutional Animal Care and Use Committee of the Helmholtz Center Munich. The paraffin-embedded lung samples were mounted onto scanning electron microscopy sample holders (PLANO GmbH, Wetzlar, Germany). The x-ray tomography experiments were performed at the beamline TOMCAT (Swiss Light Source, Paul Scherrer Institut, Villigen, Switzerland) [11]. The unstained samples were scanned two times using a 20× optical magnification (no binning, isometric voxel size of 370 nm), an exposure time of 205-230 ms per projection and an energy of 20 keV. The first scan was done at a sample detector distance of 2.5 mm (absorption contrast) and the second scan at a distance of 52.5 mm (phase contrast). Absorption contrast data sets were reconstructed using regridding techniques [11]. The modified Bronnikov algorithm was applied for the reconstruction of the phase contrast data sets [12]. 3D-visualizations were obtained using the software Imaris (Bitplane, Zürich, Switzerland). The segmentation of gold, tissue, and air was based on a global threshold of grey levels [9].

RESULTS

In the present study we developed tools for the visualization of submicron particles in the 3D-structure of the gas-exchange area of the lung. We applied 200-nm gold particles to young adult rats by intratracheal instillation. These particles were either single particles or aggregated into small clusters. The paraffin-embedded tissue was imaged unstained in order to warranty a high difference of the absorption between the gold and the alveolar septa (walls separating the alveoli). X-ray tomographic microscopy was performed at two sample detector distances. At a position very close to the detector (2.5 mm) most information was based on the absorption of the samples, and little phase information was present. We refer to it as absorption contrast. Small very bright spots, representing the gold particles, were detected in the absorption contrast images (Figs. 1a-c). As observed in serial tomographic slices, the size of the spots varied between 1-2 voxels (left circle in Figs. 1a-c) up to several voxels (right circle in Figs. 1a-c). Some of the larger particles produced spike-like artifacts (Fig. 1c). The contrast between the alveolar septa and the gold grains allowed for a segmentation of gold using a global threshold of grey levels. Even the segmentation of single, gold-containing voxels was possible (Figs. 2a-b).

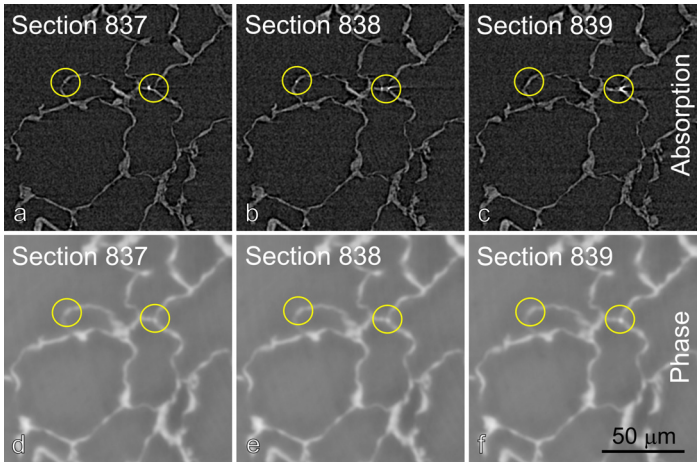

FIGURE 1. Absorption versus phase contrast. Three consecutive tomographic lung slices are shown. Absorption contrast (a-c) was used to visualize gold particles in unstained lung tissue (circles). Phase-contrast images (d-f) were used for the 3D-visualization of the alveolar septa. Voxels side length = 370 nm.

Unfortunately, this method of segmentation did not allow for a useful segmentation of the alveolar septa and the airspace (Fig. 2c), because in the absorption-contrast images the brightest voxels of the background showed higher grey values than the darkest ones of the tissue. To overcome this limitation, a second scan was recorded at a sample detector distance of 52.5 mm. In this scanning position the phase information was dominant over the absorption. The modified Bronnikov algorithm was used for the reconstructions. We refer to these data as phase contrast. The difference of the grey values between the tissue and the airspace was noticeably larger in the phase-contrast images (Fig. 1d) than in the absorption contrast images (Fig. 1a). It allowed a segmentation of the alveolar septa (Figs. 2d-f). However, using phase contrast, a segmentation of the gold particles was basically not possible.

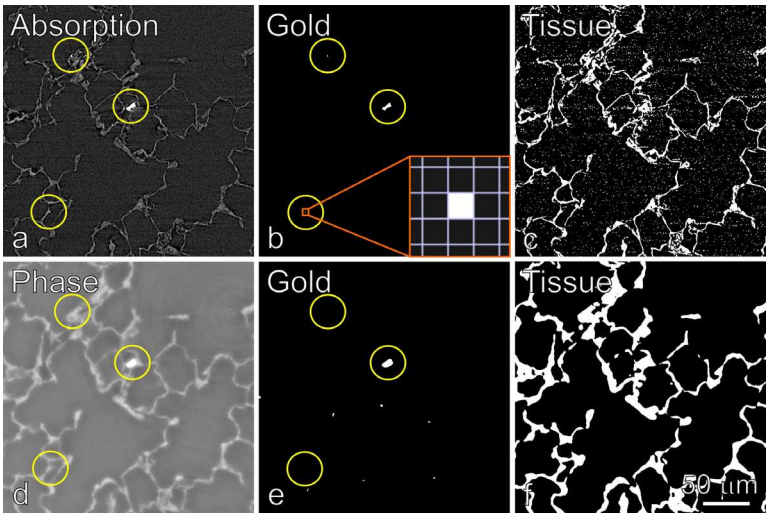

FIGURE 2. Segmentation of tissue and gold. Based on global thresholds of grey levels, a segmentation of the alveolar septa (tissue) and the gold particles was done on the absorption-contrast (a-c) and the phase-contrast images (d-f). While the segmentation of the gold particles (b+e) worked very well down to a single voxel in the absorption-contrast images (b, insert), the segmentation of the tissue (c+f) had to be done in the phase-contrast images (f). Both the segmentation of gold in the phase-contrast image (e) and tissue in the absorption-contrast image (c) resulted in an unacceptable high background signal. The original images are shown in panels a+d.

In order to localize the detected gold particles in the 3D-space of the gas-exchange area, we combined the absorption-contrast data with the phase-contrast data as two channels of one 3D data set. Due to the movement of the sample between the two scanning positions, a small voxel shift was introduced. Using gold particles as reference points, the voxel shift was corrected during the merging of the two data sets, resulting in a precise match between the two channels (Fig. 3a). The combined data sets were used to localize the gold particles in the 3D-structure of the gas-exchange area of the lung. At least at the given resolution most of the gold particles appeared to be localized inside the alveolar septa (Fig. 3b)—meaning that the uptake of the particles took less than 30 min (time between instillation of the gold suspension and fixation of the lungs).

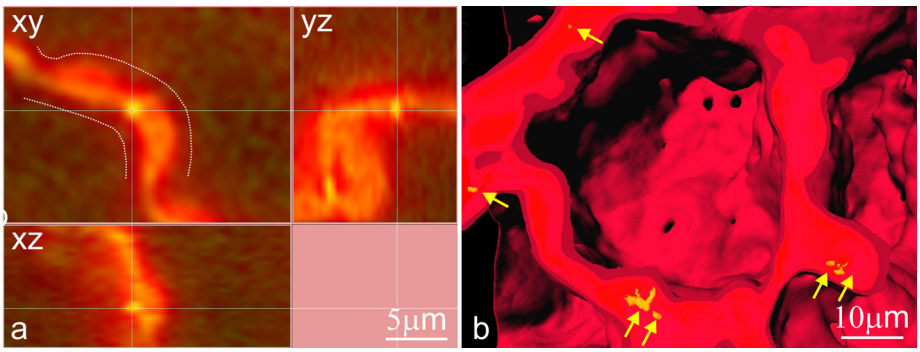

FIGURE 3. Alignment of absorption- and phase-contrast images and imaging of submicron particles in the gas-exchange area of the lung. (a) Orthogonal slices showing a gold particle (bright spots in the center of the crosshair) inside the alveolar septa. These images demonstrate the accurate alignment of the absorption-contrast (green channel) and phase-contrast images (red channel). (b) 3D view into one alveolus. Submicron gold particles (yellow, yellow arrows) were observed inside the alveolar septa (red).

CONCLUSION AND OUTLOOK

As recently shown, 700-nm gold particles were clearly identified in heavy-metal-stained lung tissue of the gas-exchange area using synchrotron-radiation-based x-ray tomographic microscopy (SRXTM) in absorption mode [13]. Although 200-nm gold particles were too small to be detected reliably in stained tissues, the introduction of phase-contrast x-ray tomographic microscopy represented a very important step. Due to the phase contrast there was no longer a need to stain the lung tissue with heavy metals because the signal-to-noise ratio of these images was sufficient for the segmentation of the tissue. As a result, gold-containing volumes were easily detectable down to the size of one voxel in the absorption-contrast images. Furthermore, the scanned tissue may be used for any kind of additional investigations; e.g., sections of paraffin-embedded tissue may be cut and used for any kind of staining, be it immunostaining or *in situ* hybridization. A registration of the stained sections in the 3D data set even allows the identification of alveoli of interest in the acinar tree of gas-exchanging airways (own unpublished data).

The smallest spots containing gold particles possessed a size of 1-2 voxels of 370-nm side length. Most likely these images represent single particles, even if we were not able to distinguish unequivocally between small clusters of 1-3 particles and single particles in the SRXTM images. An electron microscopical verification is currently being done. First results indicate that we are indeed able to detect single 200-nm gold particles. Furthermore, the fast uptake of single gold particles and small clusters was also confirmed (own unpublished data).

Our understanding of where in the pulmonary gas-exchange area particles deposit and what kind of particles these are is very limited. The combination of absorption- and phase--contrast SRXTM provides the tools to tackle this open question. We would like to take it even one step further and combine it with stereological estimations for a quantitative analysis of deposited particles. We expect that it will be possible to distinguish in 3D between areas exposed to very high or low concentrations of submicron particles.

ACKNOWLEDGMENTS

We thank Mohammed Ouanella for expert technical assistance and Drs. Federica Marone and Christoph Hintermüller for the excellent help at the beamline. This work was supported by the Swiss National Science Foundation Grant 310030-125397/1 and in part by the NIH grants HL070542, HL074022, and HL054885

REFERENCES

1. P.H. Saldiva et al., *Am. J. Resp. Crit. Care* **165**:1610 (2002).
2. K.E. Pinkerton et al., *Inhal. Toxicol.* **16** Suppl 1,73 (2004).
3. J. Sznitman, T. Heimsch, J.H. Wildhaber et al., *J. Biomech. Eng.* **131**, 031010 (2009).
4. J. Sznitman, R. Sutter, D. Altorfer, A. Tsuda, and T. Rosgen, *J. Visualization* **13**, 337 (2010).
5. S. Haber, D. Yitzhak, and A. Tsuda, *J. Appl. Physiol.* **95**, 657 (2003).
6. I. Balashazy, W. Hofmann, A. Farkas, and B.G. Madas, *Inhal. Toxicol.* **20**, 611 (2008).
7. A. Tsuda, F.S. Henry, and J.P. Butler, *J. Appl. Physiol.* **79**, 1055 (1995).
8. J. Lipka et al., *Biomaterials* **31**, 6574 (2010).
9. D. Haberthur, C. Hintermuller, F. Marone et al., *J. Synchrotron. Radiat.* **17**, 590 (2010).
10. M. Roth-Kleiner, E. Hirsch, and J.C. Schittny, J.C. Schittny, and M. Stampanoni, *Am. J. Resp. Cell. Mol.* **30**, 360 (2004).
11. C. Hintermuller, F. Marone, A. Isenegger, and M. Stampanoni, *J. Synchrotron Radiat.* **17**, 550 (2010).
12. A. Groso, R. Abela, and M. Stampanoni, *Opt. Express* **14**, 8103 (2006).
13. D. Haberthur et al., *J. Phys. Conf. Series* **186**, 012040 (2009).